Deep Self-Taught Learning for Handwritten Character Recognition

Anonymous Author(s)
Affiliation
Address
email

Abstract

Recent theoretical and empirical work in statistical machine learning has demonstrated the importance of learning algorithms for deep architectures, i.e., function classes obtained by composing multiple non-linear transformations. Self-taught learning (exploiting unlabeled examples or examples from other distributions) has already been applied to deep learners, but mostly to show the advantage of unlabeled examples. Here we explore the advantage brought by *out-of-distribution examples*. For this purpose we developed a powerful generator of stochastic variations and noise processes for character images, including not only affine transformations but also slant, local elastic deformations, changes in thickness, background images, grey level changes, contrast, occlusion, and various types of noise. The out-of-distribution examples are obtained from these highly distorted images or by including examples of object classes different from those in the target test set. We show that *deep learners benefit more from them than a corresponding shallow learner*, at least in the area of handwritten character recognition. In fact, we show that they reach human-level performance on both handwritten digit classification and 62-class handwritten character recognition.

1 Introduction

Deep Learning has emerged as a promising new area of research in statistical machine learning (see Bengio [1] for a review). Learning algorithms for deep architectures are centered on the learning of useful representations of data, which are better suited to the task at hand. This is in part inspired by observations of the mammalian visual cortex, which consists of a chain of processing elements, each of which is associated with a different representation of the raw visual input. In fact, it was found recently that the features learnt in deep architectures resemble those observed in the first two of these stages (in areas V1 and V2 of visual cortex) [2], and that they become more and more invariant to factors of variation (such as camera movement) in higher layers [3]. Learning a hierarchy of features increases the ease and practicality of developing representations that are at once tailored to specific tasks, yet are able to borrow statistical strength from other related tasks (e.g., modeling different kinds of objects). Finally, learning the feature representation can lead to higher-level (more abstract, more general) features that are more robust to unanticipated sources of variance extant in real data.

Self-taught learning [4] is a paradigm that combines principles of semi-supervised and multi-task learning: the learner can exploit examples that are unlabeled and possibly come from a distribution different from the target distribution, e.g., from other classes than those of interest. It has already been shown that deep learners can clearly take advantage of unsupervised learning and unlabeled examples [1, 5], but more needs to be done to explore the impact of *out-of-distribution* examples and of the multi-task setting (one exception is [6], which uses a different kind of learning algorithm). In particular the *relative advantage* of deep learning for these settings has not been evaluated. The hypothesis discussed in the conclusion is that a deep hierarchy of features may be better able to provide sharing of statistical strength between different regions in input space or different tasks.

In this paper we ask the following questions:

• Do the good results previously obtained with deep architectures on the MNIST digit images generalize to the setting of a much larger and richer (but similar) dataset, the NIST special database 19, with 62 classes and around 800k examples?

• To what extent does the perturbation of input images (e.g. adding noise, affine transformations, background images) make the resulting classifiers better not only on similarly perturbed images but also on the *original clean examples*? We study this question in the context of the 62-class and 10-class tasks of the NIST special database 19.

• Do deep architectures *benefit more from such out-of-distribution* examples, i.e. do they benefit more from the self-taught learning [4] framework? We use highly perturbed examples to generate out-of-distribution examples.

• Similarly, does the feature learning step in deep learning algorithms benefit more from training with moderately different classes (i.e. a multi-task learning scenario) than a corresponding shallow and purely supervised architecture? We train on 62 classes and test on 10 (digits) or 26 (upper case or lower case) to answer this question.

Our experimental results provide positive evidence towards all of these questions. To achieve these results, we introduce in the next section a sophisticated system for stochastically transforming character images and then explain the methodology, which is based on training with or without these transformed images and testing on clean ones. We measure the relative advantage of out-of-distribution examples for a deep learner vs a supervised shallow one. Code for generating these transformations as well as for the deep learning algorithms are made available. We also estimate the relative advantage for deep learners of training with other classes than those of interest, by comparing learners trained with 62 classes with learners trained with only a subset (on which they are then tested). The conclusion discusses the more general question of why deep learners may benefit so much from the self-taught learning framework.

2 Perturbation and Transformation of Character Images

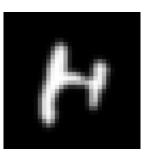

Original

This section describes the different transformations we used to stochastically transform 32×32 source images (such as the one on the left) in order to obtain data from a larger distribution which covers a domain substantially larger than the clean characters distribution from which we start. Although character transformations have been used before to improve character recognizers, this effort is on a large scale both in number of classes and in the complexity of the transformations, hence in the complexity of the learning task. More details can be found in this technical report [7]. The code for these transformations (mostly python) is available at `http://anonymous.url.net`. All the modules in the pipeline share a global control parameter ($0 \leq complexity \leq 1$) that allows one to modulate the amount of deformation or noise introduced. There are two main parts in the pipeline. The first one, from slant to pinch below, performs transformations. The second part, from blur to contrast, adds different kinds of noise.

2.1 Transformations

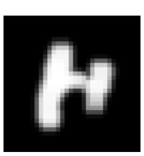

Thickness

To change character **thickness**, morphological operators of dilation and erosion [8, 9] are applied. The neighborhood of each pixel is multiplied element-wise with a *structuring element* matrix. The pixel value is replaced by the maximum or the minimum of the resulting matrix, respectively for dilation or erosion. Ten different structural elements with increasing dimensions (largest is 5×5) were used. For each image, randomly sample the operator type (dilation or erosion) with equal probability and one structural element from a subset of the $n = round(m \times complexity)$ smallest structuring elements where $m = 10$ for dilation and $m = 6$ for erosion (to avoid completely erasing thin characters). A neutral element (no transformation) is always present in the set.

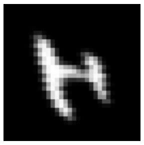

Slant

To produce **slant**, each row of the image is shifted proportionally to its height: $shift = round(slant \times height)$. $slant \sim U[-complexity, complexity]$. The shift is randomly chosen to be either to the left or to the right.

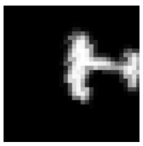

Affine Transformation

A 2×3 **affine transform** matrix (with parameters (a, b, c, d, e, f)) is sampled according to the $complexity$. Output pixel (x, y) takes the value of input pixel nearest to $(ax + by + c, dx + ey + f)$, producing scaling, translation, rotation and shearing. Marginal distributions of (a, b, c, d, e, f) have been tuned to forbid large rotations (to avoid confusing classes) but to give good variability of the transformation: a and $d \sim U[1 - 3complexity, 1 + 3\,complexity]$, b and $e \sim U[-3\,complexity, 3\,complexity]$, and c and $f \sim U[-4\,complexity, 4\,complexity]$.

!

b

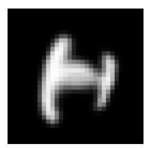

Pinch

The **pinch** module applies the “Whirl and pinch” GIMP filter with whirl set to 0. A pinch is “similar to projecting the image onto an elastic surface and pressing or pulling on the center of the surface” (GIMP documentation manual). For a square input image, draw a radius-r disk around its center C. Any pixel P belonging to that disk has its value replaced by the value of a “source” pixel in the original image, on the line that goes through C and P, but at some other distance d_2. Define $d_1 = distance(P, C)$ and $d_2 = sin(\frac{\pi d_1}{2r})^{-pinch} \times d_1$, where $pinch$ is a parameter of the filter. The actual value is given by bilinear interpolation considering the pixels around the (non-integer) source position thus found. Here $pinch \sim U[-complexity, 0.7 \times complexity]$.

2.2 Injecting Noise

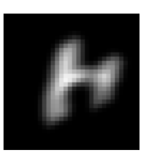

Motion Blur

The **motion blur** module is GIMP’s “linear motion blur”, which has parameters $length$ and $angle$. The value of a pixel in the final image is approximately the mean of the first $length$ pixels found by moving in the $angle$ direction, $angle \sim U[0, 360]$ degrees, and $length \sim \mathrm{Normal}(0, (3 \times complexity)^2)$.

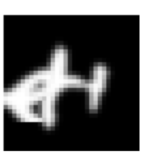

Occlusion

The **occlusion** module selects a random rectangle from an *occluder* character image and places it over the original *occluded* image. Pixels are combined by taking the max(occluder, occluded), i.e. keeping the lighter ones. The rectangle corners are sampled so that larger complexity gives larger rectangles. The destination position in the occluded image are also sampled according to a normal distribution (more details in authors [7]). This module is skipped with probability 60%.

Gaussian Smoothing

With the **Gaussian smoothing** module, different regions of the image are spatially smoothed. This is achieved by first convolving the image with an isotropic Gaussian kernel of size and variance chosen uniformly in the ranges $[12, 12 + 20 \times$

$complexity$] and $[2, 2 + 6 \times complexity]$. This filtered image is normalized between 0 and 1. We also create an isotropic weighted averaging window, of the kernel size, with maximum value at the center. For each image we sample uniformly from 3 to $3 + 10 \times complexity$ pixels that will be averaging centers between the original image and the filtered one. We initialize to zero a mask matrix of the image size. For each selected pixel we add to the mask the averaging window centered on it. The final image is computed from the following element-wise operation: $\frac{image + filtered\_image \times mask}{mask + 1}$. This module is skipped with probability 75%.

Permute Pixels

This module **permutes neighbouring pixels**. It first selects a fraction $\frac{complexity}{3}$ of pixels randomly in the image. Each of these pixels is then sequentially exchanged with a random pixel among its four nearest neighbors (on its left, right, top or bottom). This module is skipped with probability 80%.

Gauss. Noise

The **Gaussian noise** module simply adds, to each pixel of the image independently, a noise $\sim Normal(0, (\frac{complexity}{10})^2)$. This module is skipped with probability 70%.

Bg Image

Following Larochelle et al. [11], the **background image** module adds a random background image behind the letter, from a randomly chosen natural image, with contrast adjustments depending on $complexity$, to preserve more or less of the original character image.

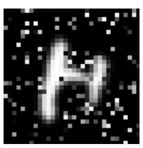

Salt & Pepper

The **salt and pepper noise** module adds noise $\sim U[0, 1]$ to random subsets of pixels. The number of selected pixels is $0.2 \times complexity$. This module is skipped with probability 75%.

Scratches

The **scratches** module places line-like white patches on the image. The lines are heavily transformed images of the digit "1" (one), chosen at random among 500 such 1 images, randomly cropped and rotated by an angle $\sim Normal(0, (100 \times complexity)^2$ (in degrees), using bi-cubic interpolation. Two passes of a grey-scale morphological erosion filter are applied, reducing the width of the line by an amount controlled by $complexity$. This module is skipped with probability 85%. The probabilities of applying 1, 2, or 3 patches are (50%,30%,20%).

Grey Level & Contrast

The **grey level and contrast** module changes the contrast by changing grey levels, and may invert the image polarity (white to black and black to white). The contrast is $C \sim U[1 - 0.85 \times complexity, 1]$ so the image is normalized into $[\frac{1-C}{2}, 1 - \frac{1-C}{2}]$. The polarity is inverted with probability 50%.

3 Experimental Setup

Much previous work on deep learning had been performed on the MNIST digits task [12, 13, 14, 15], with 60 000 examples, and variants involving 10 000 examples [16, 17]. The focus here is on much larger training sets, from 10 times to to 1000 times larger, and 62 classes.

The first step in constructing the larger datasets (called NISTP and P07) is to sample from a *data source*: **NIST** (NIST database 19), **Fonts**, **Captchas**, and **OCR data** (scanned machine printed characters). Once a character is sampled from one of these sources (chosen randomly), the second step is to apply a pipeline of transformations and/or noise processes described in section 2.

To provide a baseline of error rate comparison we also estimate human performance on both the 62-class task and the 10-class digits task. We compare the best Multi-Layer Perceptrons (MLP) against the best Stacked Denoising Auto-encoders (SDA), when both models' hyper-parameters are selected to minimize the validation set error. We also provide a comparison against a precise estimate of human performance obtained via Amazon's Mechanical Turk (AMT) service (http://mturk.com). AMT users are paid small amounts of money to perform tasks for which human intelligence is required. Mechanical Turk has been used extensively in natural language processing and vision. AMT users were presented with 10 character images (from a test set) and asked to choose 10 corresponding ASCII characters. They were forced to choose a single character class (either among the 62 or 10 character classes) for each image. 80 subjects classified 2500 images per (dataset,task) pair, with the guarantee that 3 different subjects classified each image, allowing us to estimate inter-human variability (e.g a standard error of 0.1% on the average 18.2% error done by humans on the 62-class task NIST test set).

3.1 Data Sources

NIST. Our main source of characters is the NIST Special Database 19 [18], widely used for training and testing character recognition systems [19, 20, 21, 22]. The dataset is composed of 814255 digits and characters (upper and lower cases), with hand checked classifications, extracted from handwritten sample forms of 3600 writers. The characters are labelled by one of the 62 classes corresponding to "0"-"9","A"-"Z" and "a"-"z". The dataset contains 8 parts (partitions) of varying complexity. The fourth partition (called hsf_4, 82587 examples), experimentally recognized to be the most difficult one, is the one recommended by NIST as a testing set and is used in our work as well as some previous work [19, 20, 21, 22] for that purpose. We randomly split the remainder (731668 examples) into a training set and a validation set for model selection. The performances reported by previous work on that dataset mostly use only the digits. Here we use all the classes both in the training and testing phase. This is especially useful to estimate the effect of a multi-task setting. The distribution of the classes in the NIST training and test sets differs substantially, with relatively many more digits in the test set, and a more uniform distribution of letters in the test set (whereas in the training set they are distributed more like in natural text).

Fonts. In order to have a good variety of sources we downloaded an important number of free fonts from: `http://cg.scs.carleton.ca/~luc/freefonts.html`. Including the operating system's (Windows 7) fonts, there is a total of 9817 different fonts that we can choose uniformly from. The chosen `ttf` file is either used as input of the Captcha generator (see next item) or, by producing a corresponding image, directly as input to our models.

Captchas. The Captcha data source is an adaptation of the *pycaptcha* library (a python based captcha generator library) for generating characters of the same format as the NIST dataset. This software is based on a random character class generator and various kinds of transformations similar to those described in the previous sections. In order to increase the variability of the data generated, many different fonts are used for generating the characters. Transformations (slant, distortions, rotation, translation) are applied to each randomly generated character with a complexity depending on the value of the complexity parameter provided by the user of the data source.

OCR data. A large set (2 million) of scanned, OCRed and manually verified machine-printed characters where included as an additional source. This set is part of a larger corpus being collected by the Image Understanding Pattern Recognition Research group led by Thomas Breuel at University of Kaiserslautern (`http://www.iupr.com`), and which will be publicly released.

3.2 Data Sets

All data sets contain 32×32 grey-level images (values in $[0, 1]$) associated with a label from one of the 62 character classes.

NIST. This is the raw NIST special database 19 [18]. It has {651668 / 80000 / 82587} {training / validation / test} examples.

P07. This dataset is obtained by taking raw characters from all four of the above sources and sending them through the transformation pipeline described in section 2. For each new example to generate, a data source is selected with probability 10% from the fonts, 25% from the captchas, 25% from the OCR data and 40% from NIST. We apply all the transformations in the order given above, and for each of them we sample uniformly a *complexity* in the range $[0, 0.7]$. It has {81920000 / 80000 / 20000} {training / validation / test} examples.

NISTP. This one is equivalent to P07 (complexity parameter of 0.7 with the same proportions of data sources) except that we only apply transformations from slant to pinch. Therefore, the character is transformed but no additional noise is added to the image, giving images closer to the NIST dataset. It has {81920000 / 80000 / 20000} {training / validation / test} examples.

3.3 Models and their Hyperparameters

The experiments are performed using MLPs (with a single hidden layer) and SDAs. *Hyper-parameters are selected based on the* **NISTP** *validation set error.*

Multi-Layer Perceptrons (MLP). Whereas previous work had compared deep architectures to both shallow MLPs and SVMs, we only compared to MLPs here because of the very large datasets used (making the use of SVMs computationally challenging because of their quadratic scaling behavior). The MLP has a single hidden layer with $\tanh$ activation functions, and softmax (normalized exponentials) on the output layer for estimating $P(class|image)$. The number of hidden units is taken in $\{300, 500, 800, 1000, 1500\}$. Training examples are presented in minibatches of size 20. A constant learning rate was chosen among $\{0.001, 0.01, 0.025, 0.075, 0.1, 0.5\}$.

Stacked Denoising Auto-Encoders (SDA). Various auto-encoder variants and Restricted Boltzmann Machines (RBMs) can be used to initialize the weights of each layer of a deep MLP (with many hidden layers) [12, 13, 14], apparently setting parameters in the basin of attraction of supervised gradient descent yielding better generalization [23]. It is hypothesized that the advantage brought by this procedure stems from a better prior, on the one hand taking advantage of the link between the input distribution $P(x)$ and the conditional distribution of interest $P(y|x)$ (like in semi-supervised learning), and on the other hand taking advantage of the expressive power and bias implicit in the deep architecture (whereby complex concepts are expressed as compositions of simpler ones through a deep hierarchy).

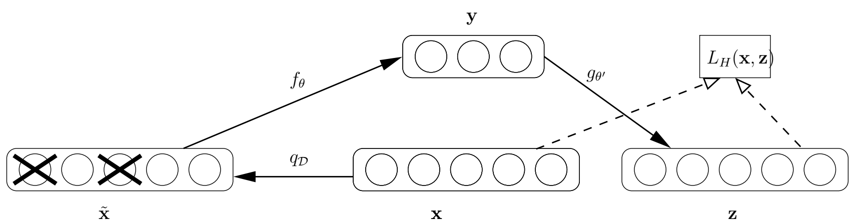

Figure 1: Illustration of the computations and training criterion for the denoising auto-encoder used to pre-train each layer of the deep architecture. Input x of the layer (i.e. raw input or output of previous layer) s corrupted into $\tilde{x}$ and encoded into code y by the encoder $f_\theta(\cdot)$. The decoder $g_{\theta'}(\cdot)$ maps y to reconstruction z, which is compared to the uncorrupted input x through the loss function $L_H(x, z)$, whose expected value is approximately minimized during training by tuning θ and θ'.

Here we chose to use the Denoising Auto-encoder [17] as the building block for these deep hierarchies of features, as it is simple to train and explain (see Figure 1, as well as tutorial and code there: `http://deeplearning.net/tutorial`), provides efficient inference, and yielded results comparable or better than RBMs in series of experiments [17]. During training, a Denoising Auto-encoder is presented with a stochastically corrupted version of the input and trained to reconstruct the uncorrupted input, forcing the hidden units to represent the leading regularities in the data. Here we use the random binary masking corruption (which sets to 0 a random subset of the inputs). Once it is trained, in a purely unsupervised way, its hidden units' activations can be used as inputs for training a second one, etc. After this unsupervised pre-training stage, the parameters are used to initialize a deep MLP, which is fine-tuned by the same standard procedure used to train them (see previous section). The SDA hyper-parameters are the same as for the MLP, with the addition of the amount of corruption noise (we used the masking noise process, whereby a fixed proportion of the input values, randomly selected, are zeroed), and a separate learning rate for the unsupervised pre-training stage (selected from the same above set). The fraction of inputs corrupted was selected among $\{10\%, 20\%, 50\%\}$. Another hyper-parameter is the number of hidden layers but it was fixed to 3 based on previous work with SDAs on MNIST [17].

4 Experimental Results

The models are either trained on NIST (MLP0 and SDA0), NISTP (MLP1 and SDA1), or P07 (MLP2 and SDA2), and tested on either NIST, NISTP or P07, either on the 62-class task or on the 10-digits task. Training (including about half for unsupervised pre-training, for DAs) on the larger datasets takes around one day on a GPU-285. Figure 2 summarizes the results obtained, comparing humans, the three MLPs (MLP0, MLP1, MLP2) and the three SDAs (SDA0, SDA1, SDA2), along with the previous results on the digits NIST special database 19 test set from the literature, respectively based on ARTMAP neural networks [19], fast nearest-neighbor search [20], MLPs [21], and SVMs [22]. More detailed and complete numerical results (figures and tables, including standard errors on the error rates) can be found in Appendix I of the supplementary material. The deep learner not only outperformed the shallow ones and previously published performance (in a

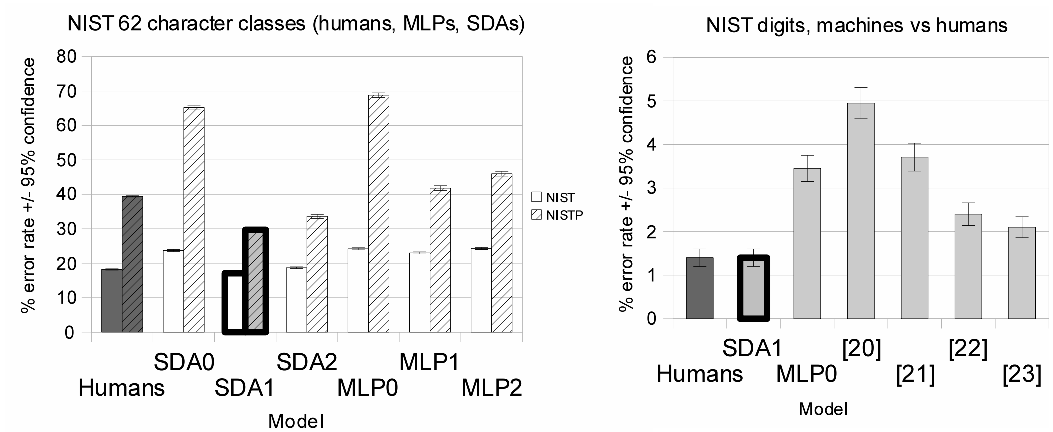

Figure 2: SDAx are the **deep** models. Error bars indicate a 95% confidence interval. 0 indicates that the model was trained on NIST, 1 on NISTP, and 2 on P07. Left: overall results of all models, on NIST and NISTP test sets. Right: error rates on NIST test digits only, along with the previous results from literature [19, 20, 21, 22] respectively based on ART, nearest neighbors, MLPs, and SVMs.

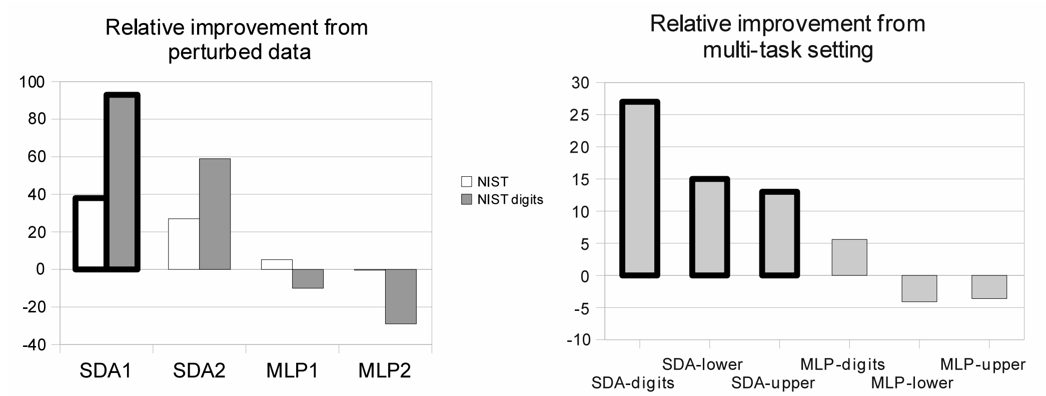

Figure 3: Relative improvement in error rate due to self-taught learning. Left: Improvement (or loss, when negative) induced by out-of-distribution examples (perturbed data). Right: Improvement (or loss, when negative) induced by multi-task learning (training on all classes and testing only on either digits, upper case, or lower-case). The deep learner (SDA) benefits more from both self-taught learning scenarios, compared to the shallow MLP.

statistically and qualitatively significant way) but when trained with perturbed data reaches human performance on both the 62-class task and the 10-class (digits) task. 17% error (SDA1) or 18% error (humans) may seem large but a large majority of the errors from humans and from SDA1 are from out-of-context confusions (e.g. a vertical bar can be a “1”, an “l” or an “L”, and a “c” and a “C” are often indistinguishible).

In addition, as shown in the left of Figure 3, the relative improvement in error rate brought by self-taught learning is greater for the SDA, and these differences with the MLP are statistically and qualitatively significant. The left side of the figure shows the improvement to the clean NIST test set error brought by the use of out-of-distribution examples (i.e. the perturbed examples examples from NISTP or P07). Relative percent change is measured by taking $100\%\times$ (original model’s error / perturbed-data model’s error - 1). The right side of Figure 3 shows the relative improvement brought by the use of a multi-task setting, in which the same model is trained for more classes than the target classes of interest (i.e. training with all 62 classes when the target classes are respectively the digits, lower-case, or upper-case characters). Again, whereas the gain from the multi-task setting is marginal or negative for the MLP, it is substantial for the SDA. Note that to simplify these multi-task experiments, only the original NIST dataset is used. For example, the MLP-digits bar shows the relative percent improvement in MLP error rate on the NIST digits test set is $100\%\times$ (single-task model’s error / multi-task model’s error - 1). The single-task model is trained with only 10 outputs (one per digit), seeing only digit examples, whereas the multi-task model is trained with 62 outputs, with all 62 character classes as examples. Hence the hidden units are shared across all tasks. For the multi-task model, the digit error rate is measured by comparing the correct digit class with the output class associated with the maximum conditional probability among only the digit classes outputs. The setting is similar for the other two target classes (lower case characters and upper case characters).

5 Conclusions and Discussion

We have found that the self-taught learning framework is more beneficial to a deep learner than to a traditional shallow and purely supervised learner. More precisely, the answers are positive for all the questions asked in the introduction.

• **Do the good results previously obtained with deep architectures on the MNIST digits generalize to a much larger and richer (but similar) dataset, the NIST special database 19, with 62 classes and around 800k examples**? Yes, the SDA *systematically outperformed the MLP and all the previously published results on this dataset* (the ones that we are aware of), *in fact reaching human-level performance* at around 17% error on the 62-class task and 1.4% on the digits.

• **To what extent do self-taught learning scenarios help deep learners, and do they help them more than shallow supervised ones**? We found that distorted training examples not only made the resulting classifier better on similarly perturbed images but also on the *original clean examples*, and more importantly and more novel, that deep architectures benefit more from such *out-of-distribution* examples. MLPs were helped by perturbed training examples when tested on perturbed input images (65% relative improvement on NISTP) but only marginally helped (5% relative improvement on all classes) or even hurt (10% relative loss on digits) with respect to clean examples . On the other hand, the deep SDAs were significantly boosted by these out-of-distribution examples. Similarly, whereas the improvement due to the multi-task setting was marginal or negative for the MLP (from +5.6% to -3.6% relative change), it was quite significant for the SDA (from +13% to +27% relative change), which may be explained by the arguments below.

In the original self-taught learning framework [4], the out-of-sample examples were used as a source of unsupervised data, and experiments showed its positive effects in a *limited labeled data* scenario. However, many of the results by Raina et al. [4] (who used a shallow, sparse coding approach) suggest that the *relative gain of self-taught learning vs ordinary supervised learning* diminishes as the number of labeled examples increases. We note instead that, for deep architectures, our experiments show that such a positive effect is accomplished even in a scenario with a *large number of labeled examples*, i.e., here, the relative gain of self-taught learning is probably preserved in the asymptotic regime.

Why would deep learners benefit more from the self-taught learning framework? The key idea is that the lower layers of the predictor compute a hierarchy of features that can be shared across tasks or across variants of the input distribution. Intermediate features that can be used in different contexts can be estimated in a way that allows to share statistical strength. Features extracted through many levels are more likely to be more abstract (as the experiments in Goodfellow et al. [3] suggest), increasing the likelihood that they would be useful for a larger array of tasks and input conditions. Therefore, we hypothesize that both depth and unsupervised pre-training play a part in explaining the advantages observed here, and future experiments could attempt at teasing apart these factors. And why would deep learners benefit from the self-taught learning scenarios even when the number of labeled examples is very large? We hypothesize that this is related to the hypotheses studied in Erhan et al. [23]. Whereas in Erhan et al. [23] it was found that online learning on a huge dataset did not make the advantage of the deep learning bias vanish, a similar phenomenon may be happening here. We hypothesize that unsupervised pre-training of a deep hierarchy with self-taught learning initializes the model in the basin of attraction of supervised gradient descent that corresponds to better generalization. Furthermore, such good basins of attraction are not discovered by pure supervised learning (with or without self-taught settings), and more labeled examples does not allow the model to go from the poorer basins of attraction discovered by the purely supervised shallow models to the kind of better basins associated with deep learning and self-taught learning.

A Flash demo of the recognizer (where both the MLP and the SDA can be compared) can be executed on-line at `http://deep.host22.com`.

References

[1] Yoshua Bengio. Learning deep architectures for AI. *Foundations and Trends in Machine Learning*, 2(1):1–127, 2009. Also published as a book. Now Publishers, 2009.

[2] Honglak Lee, Chaitanya Ekanadham, and Andrew Ng. Sparse deep belief net model for visual area V2. In *NIPS'07*, pages 873–880. MIT Press, Cambridge, MA, 2008.

[3] Ian Goodfellow, Quoc Le, Andrew Saxe, and Andrew Ng. Measuring invariances in deep networks. In *NIPS'09*, pages 646–654. 2009.

[4] Rajat Raina, Alexis Battle, Honglak Lee, Benjamin Packer, and Andrew Y. Ng. Self-taught learning: transfer learning from unlabeled data. In *ICML 2007*, pages 759–766, 2007.

[5] J. Weston, F. Ratle, and R. Collobert. Deep learning via semi-supervised embedding. In *ICML 2008*, 2008.

[6] Ronan Collobert and Jason Weston. A unified architecture for natural language processing: Deep neural networks with multitask learning. In *ICML 2008*, pages 160–167, 2008.

[7] Anonymous authors. Anonymous title. Technical report, University X., 2010.

[8] R. M. Haralick, S. R. Sternberg, and X. Zhuang. Image analysis using mathematical morphology. *IEEE Trans. Pattern. Anal. Mach. Intel.*, 9(4):532–550, 1987.

[9] J. Serra. *Image Analysis and Mathematical Morphology*. Academic Press, 1982.

[10] Patrice Simard, David Steinkraus, and John C. Platt. Best practices for convolutional neural networks applied to visual document analysis. In *ICDAR*, pages 958–962, 2003.

[11] Hugo Larochelle, Yoshua Bengio, Jerome Louradour, and Pascal Lamblin. Exploring strategies for training deep neural networks. *JMLR*, 10:1–40, 2009.

[12] Goeffrey E. Hinton, Simon Osindero, and Yee Whye Teh. A fast learning algorithm for deep belief nets. *Neural Computation*, 18:1527–1554, 2006.

[13] M. Ranzato, C. Poultney, S. Chopra, and Y. LeCun. Efficient learning of sparse representations with an energy-based model. In *NIPS'06*, 2007.

[14] Yoshua Bengio, Pascal Lamblin, Dan Popovici, and Hugo Larochelle. Greedy layer-wise training of deep networks. In *NIPS 19*, pages 153–160. MIT Press, 2007.

[15] Ruslan Salakhutdinov and Geoffrey E. Hinton. Deep Boltzmann machines. In *AISTATS'2009*, volume 5, pages 448–455, 2009.

[16] Hugo Larochelle, Yoshua Bengio, Jerome Louradour, and Pascal Lamblin. Exploring strategies for training deep neural networks. *JMLR*, 10:1–40, 2009.

[17] Pascal Vincent, Hugo Larochelle, Yoshua Bengio, and Pierre-Antoine Manzagol. Extracting and composing robust features with denoising autoencoders. In *ICML'08*, pages 1096–1103. ACM, 2008.

[18] P.J. Grother. Handprinted forms and character database, NIST special database 19. In *National Institute of Standards and Technology (NIST) Intelligent Systems Division (NISTIR)*, 1995.

[19] Eric Granger, Robert Sabourin, Luiz S. Oliveira, and Catolica Parana. Supervised learning of fuzzy artmap neural networks through particle swarm optimization. *JPRR*, 2(1):27–60, 2007.

[20] Juan Carlos Pérez-Cortes, Rafael Llobet, and Joaquim Arlandis. Fast and accurate handwritten character recognition using approximate nearest neighbours search on large databases. In *IAPR*, pages 767–776, London, UK, 2000. Springer-Verlag. ISBN 3-540-67946-4.

[21] L.S. Oliveira, R. Sabourin, F. Bortolozzi, and C.Y. Suen. Automatic recognition of handwritten numerical strings: a recognition and verification strategy. *IEEE Trans. Pattern Analysis and Mach. Intelli.*, 24(11):1438–1454, 2002.

[22] J. Milgram, M. Cheriet, and R. Sabourin. Estimating accurate multi-class probabilities with support vector machines. In *Int. Joint Conf. on Neural Networks*, pages 906–1911, 2005.

[23] Dumitru Erhan, Yoshua Bengio, Aaron Courville, Pierre-Antoine Manzagol, Pascal Vincent, and Samy Bengio. Why does unsupervised pre-training help deep learning? *JMLR*, 11:625–660, 2010.